Collaborative Control of Multiple AUVs for Improving the Estimation of Flow Field Dependent Variables

P. Axel Hackbarth and Edwin Kreuzer
Institute of Mechanics and
Ocean Engineering
Hamburg University of Technology
Hamburg, Germany
Email: {axel.hackbarth,kreuzer}@tu-hamburg.de

Andrew J. Gray and J. Karl Hedrick
Vehicle Dynamics and Control Lab
University of California
Berkeley, USA
Email: {ajgray@,hedrick@me.}berkeley.edu

***Abstract*—This paper presents a control framework for creating a 3D map of flow field dependent physical ocean variables by controlling multiple AUVs to maximize information gain. In this framework a nonlinear Kalman Filter is used to update the noisy measurements from multiple sensors at uncertain positions. First, the area of interest is discretized into a 3D grid. Each grid point has an associated estimate or measurement of the physical variable as well as its uncertainty.**

Multiple AUVs make measurements to update the value and uncertainty of the grid point at their current location. When this information is communicated between AUVs an updated 3D map is then propagated forward through time. To determine how to control the AUVs, a Nonlinear Model Predictive Controller (NMPC) is developed to generate paths for the AUVs which will minimize the overall uncertainty of the estimates in the 3D map of physical ocean variables.

Simulations are shown with multiple AUVs to illustrate the utility and application of this approach. Various fluid dynamic environments, e.g. vortex flow, are initialized, and the AUVs are controlled to optimally measure a temperature distribution. The results show this method improves the estimation of the ocean variables as well as decreases mission time when compared to naive search methods.

I. Introduction

The goal of AUV deployment is often to create a 3D map of measured physical ocean variables, such as temperature, salinity, and pollutants [1]–[3]. Environmental monitoring has become common practice in many fields to assure compliance with pollution constraints, supervise contamination after natural or anthropogenic / man-made disasters, and observe marine life. Commonly, such a map is created by a formation of AUVs following a simple pattern, such as mowing-the-lawn, through the area of interest [4]. Oftentimes this is done with static sensors that are situated in the measurement region [5]. However, this area can change due to dynamic ocean environments, i.e. convection and diffusion, thus it is beneficial to incorporate any knowledge about the flow field velocities to be able to predict how the 3D map evolves over time.

In dynamic environments static sensor nodes can only resolve a spatial distribution to a very limited resolution and cannot detect peak concentration that can exist between nodes. Autonomous mobile sensor nodes are able to dynamically adapt to the necessary measurement requirements. In [6] a mobile sensor network is presented for optimal data collection in two-dimensional environments, which is a possible simplification in many three-dimensional scenarios. Another approach has been described in [7], where multiple measurement buoys can only move in vertical direction and optimize their position to reduce the overall variance of their measurements. In [8] a path planning technique to minimize the entropy of a two-dimensional probability distribution is proposed for multiple umanned aerial vehicles. A two-dimensional approach of spatially or time-varying flow field estimation has been described in [9]. However, neither framework allowed for the optimal information gain of physical variables for multiple vehicles in a three-dimensional and dynamically changing environment.

To analyze complex flow situations, a three-dimensional data gathering technique shall be discussed in this paper. We present a framework that applies Kalman's estimation technique to flow fields with measurements from mobile sensor nodes. The position of the sensor nodes are controlled by a model predictive controller that solves an optimization problem to determine the control inputs necessary to move the sensors to a location that will minimize the overall uncertainty in the estimates of the flow field.

This paper is organized as follows: First, we describe the system in section II and give a broad overview of the components involved which are necessary to understand the later sections. In section III we derivate an algorithm to estimate the fluid field variables and their variances over time to be able to optimally integrate new measurements into the modeled field. The following section IV describes how this modeled field is used to control a mobile underwater sensor network so that new measurements are taken at positions with most valuable data for the modeled field. The performance of the control algorithm is shown with simulation results in section V. Finally the concluding remarks are described in section VI.

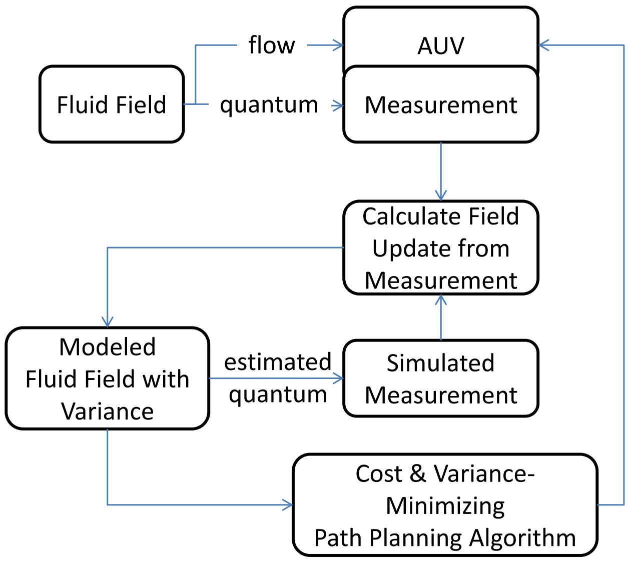

Fig. 1. System overview of real fluid environment on the top with measurement nodes (AUVs) and the modeled fluid environment on the bottom, updated through measurements from AUVs.

II. System Description

In order to monitor variables in a fluid field, the field has to be reproduced as a computer model with all necessary properties that affect the quantum of interest (e.g. flow, boundary conditions, sources). The whole system can be separated in two parts, one is the fluid domain and the other is the mobile sensor network with autonomous agents. As illustrated in figure 1, the autonomous agents move in the fluid domain and take measurements which are then used to update the model of the fluid field, which is described in detail in section III. With the knowledge about the field, the mobile sensor network is controlled in a way to expect a maximum improvement for the information of modeled field while keeping the hard and soft constraints (bounded region, collision avoidance, etc). The dynamics and control of underwater vehicles is described in section IV.

A. Fluid Field

The flow field velocities $\mathbf{u}(\mathbf{r}) = [u\ v\ w]^\top$ are assumed to be known on the whole field for this simulation and for now only time-invariant flow fields are considered. Other field variables like temperature and pollutant concentration are assumed to be independent from each other and will be represented by a generic quantum $\Theta(\mathbf{r})$.

For the control of the mobile sensor nodes the value of the quantum is in general of little interest if the whole field distribution of the quantum is supposed to be known with the least mean squared error. Instead, the variance $\mathbf{B}$ of the generic quantum Θ shall be used for each grid point as a measure of uncertainty.

B. Mobile Sensors

To dynamically adapt the measurement positions to find the best data sets, the sensors are attached to autonomous underwater vehicles that can move with respect to the vehicle dynamics through the measurement region.

The position η_j of vehicle j is estimated through various positioning techniques used in underwater robotics. When on the water surface, global navigation satellite systems gives a good absolute position estimation. While the vehicles are underwater, either an acoustic positioning system has to be installed in the region for absolute positioning, or relative measurement systems such as inertial measurement units or doppler velocity logs have to be used. All these systems yield to errors in positioning accuracy which for relative measurement systems can grow very large over long mission times.

To still be able to make use of the field measurements, this position error has to be estimated and accounted for when updating the field variables.

III. Fluid Field Estimation

The proposed system uses the method of Bayesian filters to estimate fluid dynamic environments which are analyzed by autonomous mobile sensor nodes. The model of the fluid field is therefore discretized and a Kalman Filter is used to predict and update the estimated quantum $\hat{\Theta}_k(\mathbf{r})$ and the variance $\mathbf{B}_k(\mathbf{r})$.

The system dynamics function f in Equation (8) describes the fluid field propagation of the generic quantum Θ through time:

$$\hat{\Theta}_{k|k-1}(\mathbf{r}) = f(\hat{\Theta}(\mathbf{r})_{k-1|k-1}, \mathbf{u}(\mathbf{r}))\ , \tag{1}$$

with $\mathbf{u}(\mathbf{r})$ as the flow field velocity of the fluid field.

The measurement function h of sensor node j can be subject to sensor dynamics, but for simplicity and without loss of generality we assume a direct measurement of the quantum Θ at time t_k and (uncertain) vehicle position η_j:

$$\mathbf{z}^{\Theta}_{j,k} = h(\Theta(\eta_j, t_k), \mathbf{v}_k) = \Theta(\eta_j, t_k) + \mathbf{v}_k\ . \tag{2}$$

The measurement noise $\mathbf{v}_{j,k}$ is normally distributed, zero-mean white noise with covariance matrix $\mathbf{R}_{j,k}$. The discrete measurements $\mathbf{z}^{\Theta}_{j,k}$ of the mobile sensor network are affected by the positioning uncertainty of the vehicle and the measurement uncertainty of the specific sensor. That means for each measurement variable we have a probability density function (pdf) which spans over the three spatial dimesnions and the measurement variable dimension. With a recursive Bayesian estimation algorithm it is possible to use the uncertain measurements at uncertain positions to update the predicted flow field variables optimally. Under the assumption of normally distributed noise $\mathbf{v}_{k,j}$ of the measurements from the sensor nodes j, the Bayesian estimator can be described as a nonlinear Kalman Filter.

The difference of the field measurement $\mathbf{z}^{\Theta}_{j,k}$ and an estimated measurement of the modeled field is introduced as

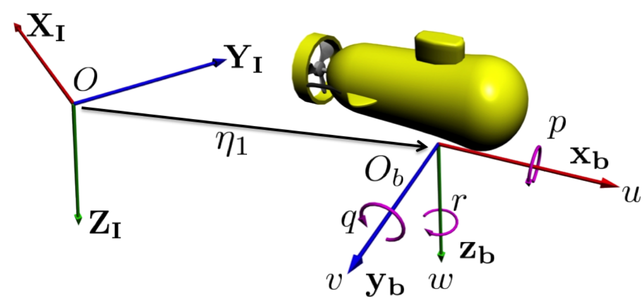

Fig. 2. A diagram of a general underwater vehicle denoting the intertial and body-fixed coordinate systems.

the innovation:

$$\mathbf{y}^{\Theta}_{j,k} = \mathbf{z}^{\Theta}_{j,k} - h(\hat{\Theta}_{j,k|k-1}, 0) \ . \tag{3}$$

With the innovation described in equation (3) we can calculate the (near)-optimal update equation for the estimated field variable $\hat{\Theta}_k(\mathbf{r})$:

$$\hat{\Theta}_k(\mathbf{r}) = \hat{\Theta}_{k|k-1}(\mathbf{r}) + \mathrm{P}(\eta_j = \mathbf{r}) \frac{\mathbf{y}^{\Theta}_{j,k}}{1 + \mathbf{R}_{j,k}/\mathbf{B}_{k|k-1}(\mathbf{r})} \ , \tag{4}$$

where $\mathrm{P}(\eta_j = \mathbf{r})$ denotes the probability of sensor j being at position $\mathbf{r}$ in the fluid field. This probability distribution can be nonlinear and multimodal, but for most positioning techniques a Gaussian distribution is a sufficiently good approximation [10].

The variance $\mathbf{B}_k(\mathbf{r})$ of the field variable Θ can be determined similarly for each position $\mathbf{r}$ in the fluid field and each sensor node j :

$$\mathbf{B}_k(\mathbf{r}) = \mathbf{B}_{k|k-1}(\mathbf{r}) + \mathrm{P}(\eta_j = \mathbf{r}) \frac{\mathbf{R}_{j,k} + \mathbf{B}_{k|k-1}(\mathbf{r})}{(1 + \mathbf{R}_{j,k}/\mathbf{B}_{k|k-1})^2} \ . \tag{5}$$

The variance is used as an element of the cost function of the AUVs described in the following section.

IV. Path Planning of Mobile Sensors

A. Underwater Vehicle Dynamics

The vehicle dynamics are briefly introduced here for sake of completeness, we refer the reader to [10] for further details. Consider the vehicle sketch in figure 2. The differential equations are written in the following compact form:

$$\mathbf{M}\dot{\nu} + \mathbf{C}(\nu) + \mathbf{D}(\nu) + g(\eta) = \tau \tag{6a}$$
$$\dot{\eta} = \mathbf{J}(\eta)\nu \tag{6b}$$

where ν is the body-fixed velocities and angular velocities, $\nu = [u, v, w, , p, q, r]^T \in \mathbb{R}^6$ and η is the inertial positions and angles, $\eta = [x, y, z, , \phi, \theta, \psi]^T \in \mathbb{R}^6$. The system matrices are defined as:

$$\mathbf{M} = \mathbf{M}_{RB} + \mathbf{M}_A$$
$$\mathbf{C}(\nu) = \mathbf{C}_{RB}(\nu) + \mathbf{C}_A$$
$$\mathbf{D} = \mathbf{D}_{\text{quad}} + \mathbf{D}_{\text{lin}}$$

where $\mathbf{M} \in \mathbb{R}^{6\times6}$ is the rigid body mass and *added mass* matrix, $\mathbf{C} \in \mathbb{R}^{6\times6}$ is the Coriolis and centripetal matrix, and $\mathbf{D} \in \mathbb{R}^{6\times6}$ is the quadratic and linear hydrodynamic damping matrix. The vector $g(\eta) \in \mathbb{R}^6$ is the restoring forces and $\tau \in \mathbb{R}^6$ is the external forces and moments acting on the vehicle, including those of the actuators, denoted as u . Finally, $\mathbf{J}(\eta)$ is the rotation matrix from inertial to body-fixed angular velocities.

For the predictive control problem formulation we write the nonlinear dynamics in standard first-order form

$$\dot{\xi}(t) = f(\xi(t), u(t)) \tag{8}$$

where $\xi = [\nu, \eta]$ and the state of the vehicle at time t is $\xi(t)$ and the control input $u(t)$ is the contribution from the actuators in the force vector τ . We note the following assumptions:

Assumption 1: The vehicle is completely submerged, traveling at low velocity, has three planes of symmetry, and has constant coeficients.

Assumption 2: The body-fixed frame is chosen to be coincident with the principal axes, i.e. $I_{xz} = I_{yz} = I_{xy} = 0$.

B. Constraints

We address the physical limitations of the vehicle actuators and the system dynamics by formulating constraints on the vehicle's inputs and states. The hard contraint on the vehicle's actuators are expressed as

$$u_{\min} \leq u \leq u_{\max} \tag{9}$$

In addition, the change rate of the vehicle's actuators are limited and expressed as

$$\Delta u_{\min} \leq \Delta u \leq \Delta u_{\max} \tag{10}$$

The vehicle state, ξ , is also contrained to lie within the boundary region of interest, to avoid any underwater topology construction, and to avoid collisions with other vehicles. These requirements can be compactly written as

$$h(\xi, u) \leq \mathbf{0} \tag{11}$$

where $\mathbf{0}$ is a vector of zeros with appropriate dimension.

C. Cost Function and Potential Fields

The cost is defined from an agent's perspective. Consequently, forbidden zones and other vehicles' paths and regions that have been well explored have a high cost so that the agent avoids it. On the other hand, unexplored regions with a high uncertainty have a very low cost, thereby attracting agents. In [11] these so-called virtual repulsive and attractive potentials have been applied for cooperative guidance control of aerial vehicles in two dimensions.

Furthermore, the different cost maps can be categorized into global maps that are valid for all agents and local maps which are only valid for a specific agent. The global maps document the mission achievements, which are the level of exploration of the region, and the uncertainty of the targets.

The field information of the region is the inverse of the variance matrix (5).

$$\mathbf{K}_{region} = \mathbf{B}_k^{-1} \ . \tag{12}$$

We define the information gain as the difference in overall posterior estimated region knowledge $\hat{\mathbf{K}}_{k+1}$ and the current belief $\mathbf{K}_k$

$$J_i = \hat{\mathbf{K}}_{k+1} - \mathbf{K}_k \ , \tag{13}$$

To avoid collisions with other agents, they are modeled as repulsive $1/x^2$ function:

$$J_a(\eta) = \sum_{agents \neq j} \left\|(\eta_j - \eta_{agents})\right\|^{-2} \ . \tag{14}$$

Additional potential layers for specific tasks can easily be included and hence gives a high flexibility to various scenarios, but with a high number of cost functions the mission objective might become unclear and can result in bad decisions of the AUVs.

The cost function J_j is the information gain (13) added with the sum of the cost J_j^i of all tasks that need to be considered by vehicle j at time step t :

$$J_j(\eta, t) = \sum_i \alpha_i J_j^i(\eta, t) \ , \tag{15}$$

where α_i is a runtime-alterable weighting factor for scaling and setting the importance of the individual task i .

D. Predictive Control Problem

In this section we formulate the control problem of each underwater vehicle as a Model Predictive Control Problem (MPC). At each sampling time instant an optimal input sequence is calculated by solving a constrained finite time optimal control problem. The computed optimal control input sequence is only applied to the vehicle during the following sampling interval. At the next time step the optimal control problem is solved again, using new measurements.

We discretize the system (8) with a fixed sampling time T_s for vehicle j to obtain:

$$\xi_{k+1}^j = f^{j,d}(\xi_k, u_k,), \tag{16}$$

and formulate the optimization problem, to be solved at each time instant, as:

$$\min_{\mathcal{U}_t, \epsilon} \sum_{k=t}^{t+H_p-1} J_j(\eta, t) + \rho\epsilon \tag{17a}$$

$$s.t. \ \xi_{t+k+1,t} = f^d(\xi_{t+k,t}, u_{t+k,t}), \quad k = t, ..., t+H_p-1 \tag{17b}$$

$$h_t(\xi_{t+k,t}, u_{t+k,t}) \leq \mathbf{1}\epsilon, \tag{17c}$$

$$\epsilon \geq 0, \qquad k = t, ..., t+H_p-1 \tag{17d}$$

$$u_{t+k,t} = \Delta u_{t+k,t} + u_{t+k-1,t}, \tag{17e}$$

$$u_{\min} \leq u_{t+k,t} \leq u_{\max}, \tag{17f}$$

$$\Delta u_{\min} \leq \Delta u_{t+k,t} \leq \Delta u_{\max}, \quad k = t, ..., t+H_p-1 \tag{17g}$$

$$u_{t-1,t} = u(t-1), \tag{17h}$$

$$\xi_{t,t} = \xi(t), \tag{17i}$$

where the cost for vehicle J_j is defined in equation (15), t denotes the current time instant and $\xi_{t+k,t}$ denotes the predicted state at time $t+k$ obtained by applying the control sequence $\mathcal{U}_t = [u_{t,t}, \ldots, u_{t+k,t}]$ to the system (8) with $\xi_{t,t} = \xi(t)$. H_p denotes the prediction horizon. The safety constraints (11) have been imposed as soft constraints, by introducing the slack variable ϵ in (17a) and (17d). ρ is a scalar weight penalizing the violation of the soft constraints. In addition to the soft constraints we have imposed hard constraints. (17e)-(17g) reflect limitations set by the actuators.

This is a non-convex nonlinear optimization problem and we use a Matlab implementation of the commercial package NPSOL [12] to solve the problem. With a prediction horizon of $H_p = 15$ and a grid size of $65 \times 43 \times 16$ it takes on average 20 sec. to converge for each vehicle.

V. Simulation Results

In this section we describe the performance and the behavior of the developed algorithm on two different example flow field environments. All simulations were conducted with a time step of $1\mathrm{s}$ and a vehicle velocity of $1\frac{\mathrm{m}}{\mathrm{s}}$.

The first simulation was done in a three-dimensional environment, but for better illustration we kept the third dimension very shallow so it behaves almost like a two-dimensional system (cf. figures 3). The grid size is $40 \times 40 \times 2$. The blue lines represent streamlines of the flow field which are always parallel to the flow velocity with a mean of $0.3\frac{\mathrm{m}}{\mathrm{s}}$. The distance between the blue streamlines is proportional to the velocity of the two-dimensional vortex flow field. The green lines show the position, heading and velocity of the vehicles with the center of mass being at the intersection of the lines. Magenta circles symbolize the predicted optimal path with the planning horizon length. The background color shows the belief of the information we have found out through measurement in that region. The whole map is initially black, stating that we have no information and the field variance (see section III equation (5)) is infinitely large. As the agents move around, this map is filled with information where the agents take measurements. On a scale from black over green and yellow to red the belief in the estimate of the field variable $\hat{\Theta}_k(\mathbf{r})$ is shown, described by the inverse of the variance $\mathbf{B}_k(\mathbf{r})$ described in equation (5). Red stands for the information we get from a good sensor measurement with average positioning uncertainty.

Figure 3a shows the stage right after the start of the vehicles heading out with a small time delay between each vehicle. At this time, the region information as the inverse of the field variance increases linearly over time as can be seen in figure 4. As time continues, the variance gain slows down and in the final stage (cf. figure 3d) the variance is almost everywhere at a value of the sensor accuracy which is illustrated in red color.

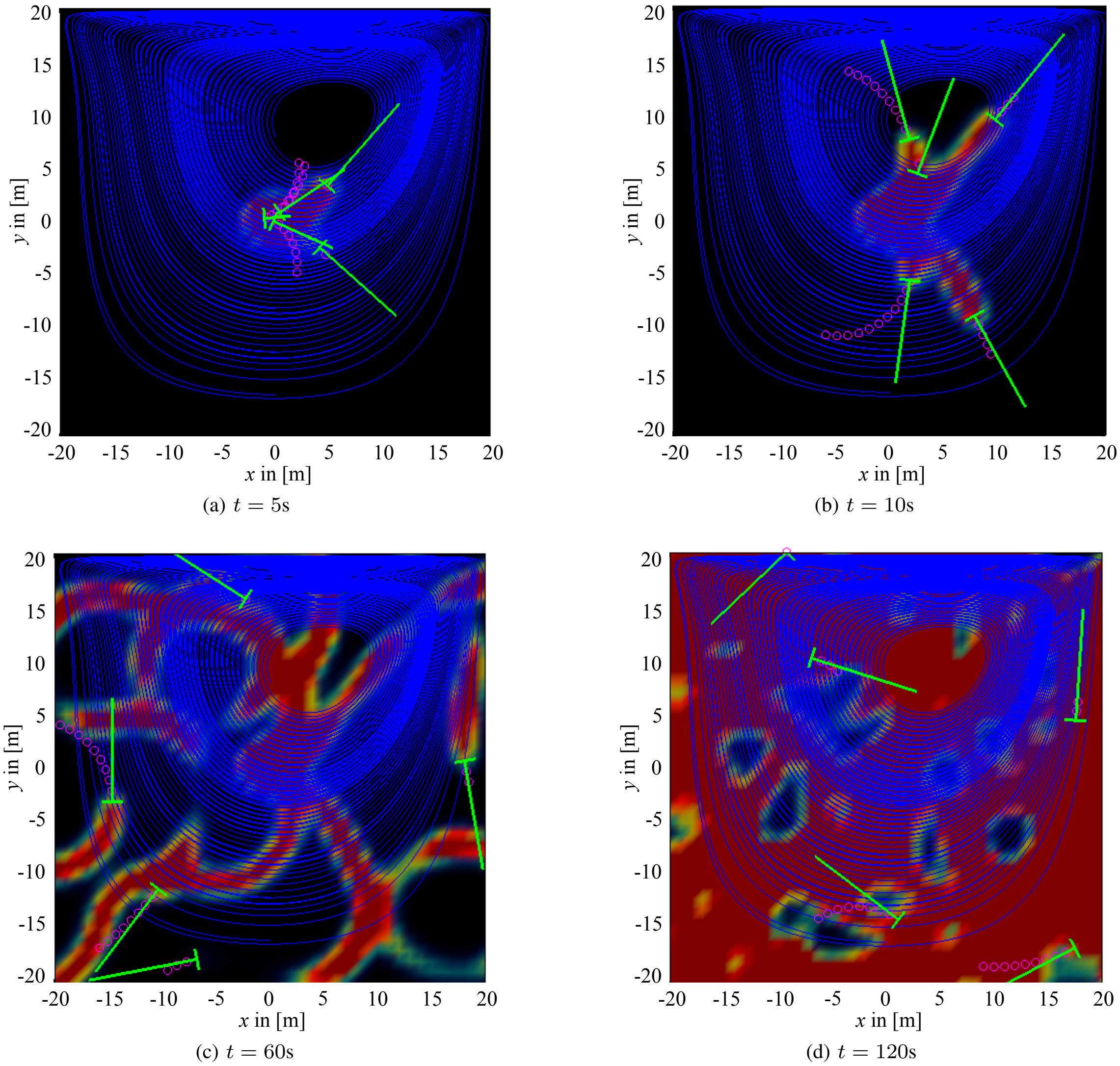

(a) $t = 5\text{s}$ (b) $t = 10\text{s}$ (c) $t = 60\text{s}$ (d) $t = 120\text{s}$

Fig. 3. The figures show a slice of the region information ($\mathbf{B}^{-1}$), defined in equation (5)) of the three-dimensional field (which for this illustration is kept shallow in one direction). The green lines show agents with their planned paths as magenta circles (1 circle per time step of 1s and a velocity of $1\frac{\text{m}}{\text{s}}$). Blue lines illustrate stream lines of the flow case, here a standard CFD test scenario with a horizontal velocity at the upper edge of 1m/s, which is affecting the fluid field (average velocity of $0.3\frac{\text{m}}{\text{s}}$) and thereby the vehicle dynamics. In (a) and (b) the swarm of five vehicles distributes quickly into directions after starting from the same position with the same heading. (c) and (d) show the simulation in the final stage when most of the region has already been searched.

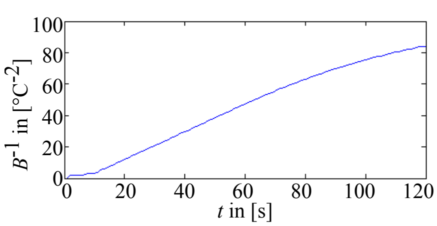

Fig. 4. This plot shows the information gain over time of the vortex simulation (cf. figure 3). It clearly shows the expected behavior when all agents start from the same initial position, thereby producing redundant measurements in the beginning. from 10 to 70 seconds, the graph shows an approximately linear increase in information due to an initially unknown field. After 70 seconds the information gain decreases because the area has been well explored and the mean variance is close to the sensor noise.

Due to the limited prediction horizon H_p the performance degrades in the final stages because the planned paths are only locally optimal and do not reach areas with high variance. We note a variable length receding horizon has the potential to increase performance when the variance appears flat.

In the second example (cf. figures 5) a turbulent flow entering on the left side with a mean of $0.5\frac{\text{m}}{\text{s}}$ and leaving the region on the right side. The region is discretized by $42 \times 64 \times 16$ cells and since it is not possible to illustrate the whole three-dimensional field, the field information is shown only as the projection onto the three perpendicular back planes.

In figure 5a it can be seen that the model predictive controller makes use of the flow field and follows the wind to minimize control input with three agents distributing in the vertical axis to prevent redundant measurements.

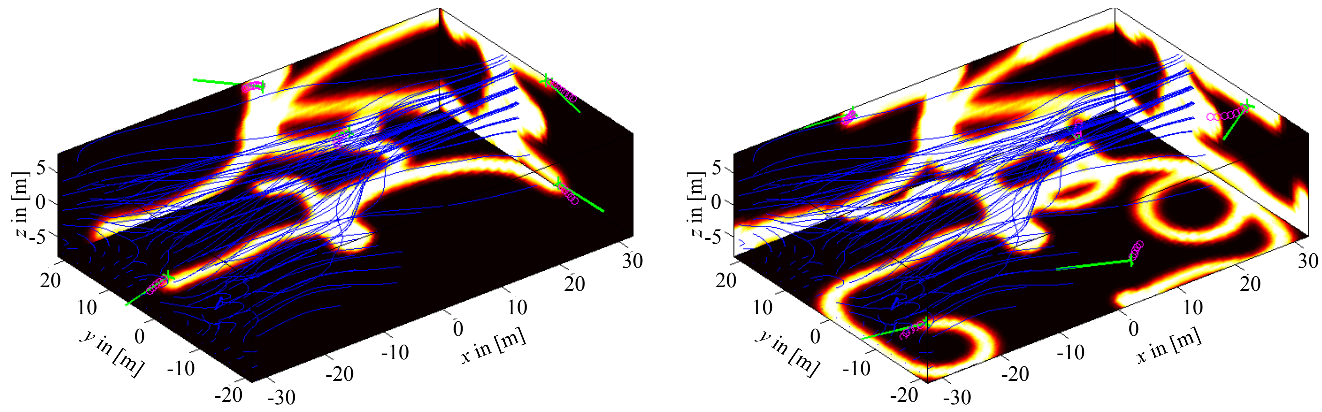

(a) $t = 30$s

(b) $t = 90$s

Fig. 5. Open turbulent 3D scenario: flow is entering on the left side and is passing to the right, illustrated by the blue streamlines. The uncertainty of the 3D field is projected on the three back planes and colored with a gradient from black over red and yellow to white for visualization, where black represents a high variance and white is close to the sensor resolution.

VI. Conclusion

This paper presented a multi-agent control algorithm that reproduces a real fluid environment through measurements into a model thereof, which is continuously updated and used for the path planning algorithm for the multi-agent sensor network. Due to the flexible potential field based cost function, different side-tasks can be assigned to the vehicle, like maintaining communication range or manually defining high areas of interest in mission time.

The agents were modeled as underactuacted underwater vehicles with nonlinear dynamics and active propulsion in longitudinal and vertical direction. Including different underwater vehicles, also as a heterogeneous network, does not pose any complications for the control algorithm.

The processing of sensor measurements has been implemented with the technique of nonlinear Kalman Filtering, which can on the one hand estimates the current condition of the field variables through forward propagation of estimated current belief, on the other hand finds an optimal correction term to feed back the new sensor measurement and integrate it with prior knowledge of the field. A nonlinear model predictive controller was developed that calculates the control inputs necessary to move the agents such that future measurements will minimize the uncertainty in the flow field's estimates, thus maximizing the information gain.

We further intend to use this framework to propagate fluid field velocities including the propagation and degradation of the belief in all variables over space and time. Thereby we will be able to optimally plan the trajectories of multiple mobile sensor nodes in an uncertain time-varying fluid flow field.

References

[1] E. Fiorelli, N. Leonard, P. Bhatta, D. A. Paley, R. Bachmayer, and D. Fratantoni, "Multi-AUV control and adaptive sampling in Monterey Bay," in *2004 IEEE/OES Autonomous Underwater Vehicles (IEEE Cat. No.04CH37578).* IEEE, 2004, pp. 134–147.

[2] G. Antonelli, T. I. Fossen, and D. R. Yoerger, "Underwater Robotics," in *Springer Handbook of Robotics*. Berlin, Heidelberg: Springer Berlin Heidelberg, 2008, pp. 987–1008.

[3] A. Jarre-Teichmann, T. Brey, U. V. Bathmann, C. Dahm, G. S. Dieckmann, M. Gorny, M. Klages, F. Pagès, J. Plötz, S. B. Schnack-Schiel, M. Stiller, and W. E. Arntz, "Trophic flows in the benthic shelf community of the eastern Weddell Sea, Antarctica," in *Antarctic communities: Species, structure and survival*, B. Battaglia, J. Valencia, Walton, and D.W.H., Eds. Cambridge: Cambridge Univ Press, Jan. 1997.

[4] J. Kalwa and M. Jarowinsky, "Underwater robotic cooperation," *Schiff & Hafen*, no. 05/09, pp. 46–48, May 2009.

[5] F. Monaldo, D. Thompson, R. Beal, W. Pichel, and P. Clemente-Colon, "Comparison of SAR-derived wind speed with model predictions and ocean buoy measurements," *IEEE Transactions on Geoscience and Remote Sensing*, vol. 39, no. 12, pp. 2587–2600, 2001.

[6] N. Leonard, D. A. Paley, F. Lekien, R. Sepulchre, D. Fratantoni, and R. Davis, "Collective Motion, Sensor Networks, and Ocean Sampling," *Proceedings of the IEEE*, vol. 95, no. 1, pp. 48–74, 2007.

[7] C. Detweiler, M. Doniec, M. Jiang, M. Schwager, R. Chen, and D. Rus, "Adaptive decentralized control of underwater sensor networks for modeling underwater phenomena," in *Proceedings of the 8th ACM Conference on Embedded Networked Sensor Systems*, ser. SenSys '10. New York, NY, USA: ACM, 2010, pp. 253–266.

[8] J. Tisdale, Z. Kim, and J. Hedrick, "Autonomous UAV path planning and estimation," *IEEE Robotics & Automation Magazine*, vol. 16, no. 2, pp. 35–42, Jun. 2009.

[9] C. Peterson and D. A. Paley, "Multivehicle Coordination in an Estimated Time-Varying Flowfield," *Journal of Guidance, Control, and Dynamics*, vol. 34, no. 1, pp. 177–191, Jan. 2011.

[10] T. I. Fossen, *Handbook of Marine Craft Hydrodynamics and Motion Control*. Wiley-Blackwell, 2011.

[11] A. Hackbarth, J. K. Hedrick, and E. Kreuzer, "A Multi-Layered Potential Field Method for Multi-Agent Navigation, Searching and Tracking," in *PAMM 2010 Karlsruhe*, C. Wieners, Ed., vol. 10, no. 1. Weinheim: Wiley-VCH, Dec. 2010, pp. 609–610.

[12] P. E. Gill, W. Murray, M. A. Saunders, and M. H. Wright, "NPSOL Nonlinear Programming Software," Mountain View, CA, 1998.